Lawrence Berkeley National Laboratory
LBL Publications

Title

STATISTICAL ANALYSIS OF CLEAVAGE FRACTURE AHEAD OF SHARP CRACKS AND ROUNDED NOTCHES

Permalink

https://escholarship.org/uc/item/3zp2w99t

Authors

Lin, T.
Evans, A.G.
Ritchie, R.O.

Publication Date

1985-12-01

Lawrence Berkeley Laboratory

UNIVERSITY OF CALIFORNIA

Materials & Molecular Research Division

STATISTICAL ANALYSIS OF CLEAVAGE FRACTURE
AHEAD OF SHARP CRACKS AND ROUNDED NOTCHES

T. Lin, A.G. Evans and R.O. Ritchie

December 1985

DISCLAIMER

This document was prepared as an account of work sponsored by the United States Government. While this document is believed to contain correct information, neither the United States Government nor any agency thereof, nor the Regents of the University of California, nor any of their employees, makes any warranty, express or implied, or assumes any legal responsibility for the accuracy, completeness, or usefulness of any information, apparatus, product, or process disclosed, or represents that its use would not infringe privately owned rights. Reference herein to any specific commercial product, process, or service by its trade name, trademark, manufacturer, or otherwise, does not necessarily constitute or imply its endorsement, recommendation, or favoring by the United States Government or any agency thereof, or the Regents of the University of California. The views and opinions of authors expressed herein do not necessarily state or reflect those of the United States Government or any agency thereof or the Regents of the University of California.

STATISTICAL ANALYSIS OF CLEAVAGE FRACTURE

AHEAD OF SHARP CRACKS AND ROUNDED NOTCHES

by

Tsann Lin,[1] A. G. Evans,[2] and R. O. Ritchie[1]

[1]Materials and Molecular Research Division
Lawrence Berkeley Laboratory
and
Department of Materials Science and Mineral Engineering
University of California, Berkeley, CA 94720

[2]Materials Group, College of Engineering,
University of California, Santa Barbara, CA. 93106

December 1985

accepted by <u>Acta Metallurgica</u>

STATISTICAL ANALYSIS OF CLEAVAGE FRACTURE
AHEAD OF SHARP CRACKS AND ROUNDED NOTCHES

Tsann Lin,[1] A. G. Evans, [2] and R. O. Ritchie[1]

[1]Materials and Molecular Research Division
Lawrence Berkeley Laboratory, and
Department of Materials Science and Mineral Engineering
University of California, Berkeley, CA

[2]Materials Group, College of Engineering,
University of California, Santa Barbara, CA

ABSTRACT

Mechanisms of initiation and unstable propagation of transgranular cleavage cracks are compared for brittle fracture ahead of sharp cracks and rounded notches, e.g., for fatigue pre-cracks and Charpy V-notches, respectively, in standard toughness specimens. The comparison is made over a range of temperatures, from the lower shelf into the ductile/brittle transition region, for a single phase material containing a known distribution of particles where weakest link statistics can be used to model the onset of catastrophic failure. Using linear and nonlinear elastic solutions for the stress distribution ahead of a sharp crack, and slip-line field solutions, modified for a power hardening material, for the rounded notch, statistical modelling is employed to define the critical dimensions ahead of the crack or notch tip where initial cracking events are most probable. The analysis provides an interpretation of the role of stress gradient in governing microscopic fracture behavior. Predictions are evaluated by comparison with experimental results on the low temperature flow, Charpy V-notch and plane strain fracture toughness behavior of a low carbon mild steel with simple ferrite/grain boundary carbide microstructures.

NOMENCLATURE

a	crack, or notch, length
b	characteristic dimension along crack front
B	test piece thickness
c_1, c_2	constants describing equivalent notch strain field
d_g	average grain diameter
d_p	diameter of cracked particle
D_1, D_2	functions of $\bar{\varepsilon}_t/\varepsilon_0$ and r/ρ, respectively, defined in Eq. (11)
E	Young's modulus
f	"eligibility" factor in Eq. (4)
g(S)dS	elemental strength distribution of particles
I_n	dimensionless parameter in HRR singular solution
J_{Ic}	plane strain fracture toughness (critical value of J-integral at fracture)
K_I	stress intensity factor (Mode I)
K_{Ic}	plane strain fracture toughness (critical value of K_I at fracture)
L	loading span in four-point bend specimen
m	shape factor in Weibull assumption
n	work hardening exponent ($1 < n < \infty$)
N_0	number of particles per unit volume
P	applied load
r, Θ	polar coordinates with origin at crack tip or notch center
r_c	distance from notch center where $r \sim 2.3\rho$
r_{max}	location of peak stress from crack tip or notch center

r_y	plastic zone size
r^*	distance from tip where $d\delta\varphi = 0$
r_f^*	radial characteristic distance from tip (at $K_I = K_{Ic}$)
s, t	functions defined in Eq. (13)
S	fracture strength of particle
S_0	scale parameter in Weibull assumption
S_u	fracture strength of largest observable particle
$\Delta V, V$	elemental and total active zone volume, respectively
W	test piece width
α, β	characteristic coordinates for lines of maximum shear stress
γ_p	"effective" fracture surface energy
δ	crack tip opening displacement
$\bar{\varepsilon}_t$	equivalent strain at notch tip
ζ	factor describing boundary of slip-line field
ξ	function in Eq. (23)
ν	Poisson's ratio
η	function in Eq. (23)
ρ	root radius of notch
σ	local stress within plastic zone
σ^*	local stress where $d\delta\varphi = 0$
$\bar{\sigma}, \bar{\varepsilon}$	equivalent stress and strain, respectively
σ_1	maximum principal stress
σ_f^*	cleavage fracture stress
$\tilde{\sigma}$	function in HRR crack tip field singular solution
σ_{nom}	nominal bending stress

σ_0, ε_0 flow (or yield) stress and strain, respectively

$\delta\varphi, \Phi$ elemental and total failure probabilities, respectively

ω $\alpha - \beta$

I. INTRODUCTION

Classically, material toughness has been assessed in terms of the energy absorbed during the fracture of small rounded notched specimens. Prominent among such tests is the Charpy V-notch impact test (1). More recently, quantitative assessment of toughness has been achieved through plane strain measurements of the critical stress intensity and J-integral, i.e., K_{Ic} and J_{Ic}, respectively, for the initial extension of a microscopically-sharp flaw (2,3).

Although the fracture toughness parameters, K_{Ic} and J_{Ic}, are far more amenable to engineering design calculations, they are subject to many strict measurement requirements (2,3) and thus are considerably more expensive to determine. Accordingly, for many applications, involving ship and bridge steels for example, there have been numerous attempts to correlate Charpy V-notch toughness with K_{Ic} and J_{Ic}, as reviewed for example in ref. 4. Such correlations invariably are empirical (and often dimensionally incorrect), but may provide an inexpensive and reasonably accurate means of estimating K_{Ic} values from sub-size samples (at least on materials for which explicit correlations have been established).

Despite the widespread use of these correlations, certain "anomalies" have been reported in recent years (5). For example, in low alloy 4340-type steels, it has been shown that "sharp crack" K_{Ic} toughness can be **increased** as the coarseness of the microstructure is increased by raising the austenitizing temperature, while the "rounded-notch" Charpy values actually **decreased** (6,7), a result

1

independent of loading rate and fracture mode (5-7). Another example involves wrought and cast steels, for which Charpy V-notch measurements implied an inferior toughness of cast alloys, whereas K_{Ic} values remained unchanged (8).

These discrepancies result primarily from the larger critical volume of stressed material involved in the fracture process ahead of a rounded notch, compared to that ahead of a sharp crack, resulting in major differences in extent of the fracture "process zone" compared with the characteristic microstructural size. This difference in scale derives from distinct differences in form of the stress field local to the crack (or notch) tip (9,10), and specifically to the location of maximum local tensile (and hydrostatic) stresses. This location dictates whether the stress distribution ahead of the tip is increasing or decreasing over dimensions comparable with the microstructural scale of fracture events (Fig. 1).

The objective of the present paper is to present a new micro-mechanical analysis for transgranular cleavage ahead of a rounded notch, using a recently developed weakest link statistical model (11), and to compare results with that for fracture ahead of a sharp crack. The analysis is performed for a single phase microstructure, containing a known distribution of grain boundary particles, as the crack nuclei. Predictions of the local fracture stress, characteristic distance and cleavage fracture toughness are compared with low temperature experimental results on a low carbon mild steel.

2

II. STATISTICAL RELATION FOR TRANSGRANULAR CLEAVAGE

The process of cleavage fracture is envisioned in terms of the slip-induced cracking of predominately grain boundary particles, followed by propagation of the resultant cracks into the surrounding matrix (12,13). Ahead of a rounded notch (with root radius large compared to microstructural dimensions), this process has been considered to occur when the maximum value of the local tensile stress exceeds a critical fracture stress (14), generally regarded as a quantity independent of temperature and strain rate (14,15). For loads well below general yield, the location of the peak stress ahead of a notch (Fig. 1a) (10,16) suggests that the initial cracking event in notched specimens occurs at a distance the order of the plastic zone size ahead of the notch tip. Conversely, for cleavage fracture ahead of a microscopically-sharp crack, the maximum tensile stresses occur far closer to the tip within two crack tip opening displacements (Fig. 1b) (9), leading to the Ritchie, Knott and Rice (RKR) postulate that the local tensile stresses must exceed the fracture stress over a microstructurally-significant (characteristic) distance ahead of the crack tip (17).

In stochastic terms, these models can be re-formulated using weakest link statistics (11,18-22). Accordingly, the cleavage fracture toughness is estimated in terms of the volume of material within the plastic zone needed to assure the presence of an "eligible" cracked particle, at which the fracture criterion is

satisfied. The probability of finding an "eligible" particle is promoted with increasing volume, i.e., with increasing distance from the tip. Consequently, the site of the critical fracture event is dictated by the local stress gradient over the relevant microstructural size-scales: positive for the rounded notch, but negative for the sharp crack.

The statistical model considers that particles located within the plastic zone are susceptible to cracking and, when cracked, exhibit a "strength" S inversely related to their diameter d_p (23),

$$S^2 = \frac{\pi E \gamma_p}{(1 - \nu^2)d_p} \tag{1}$$

where E is Young's modulus, ν is Poisson's ratio, and γ_p is the effective fracture surface energy of the matrix. The plastic zone volume is characterized in terms of active elements, located distance r from the tip, of volume δV given by (11):

$$\delta V = 2b \int_0^\pi r \delta r \, d\Theta \quad , \tag{2}$$

where b is a characteristic dimension describing the distance between initial nucleation events **along the crack front** (19). Such elements represent regions of constant stress in which particle microcracks liable to be activated all have strengths less than, or equal to, the appropriate local stress σ. The total failure probability can then be stated in terms of the elemental particle strength distribution g(S)dS and the product of the survival probabilities of all elements

4

integrated over the plastic zone (24):

$$\Phi = 1 - \exp\left\{-\int_0^V \left[dV \int_0^\sigma g(S)dS\right]\right\} \quad . \tag{3}$$

The number of cracked particles in a unit volume having strengths between S and S+dS, g(S)dS, can be evaluated using the three-parameter Weibull assumption (25):

$$\int_0^\sigma g(S)dS = \left(\frac{\sigma - S_u}{S_0}\right)^m fN_0 \quad , \tag{4}$$

where m is a shape factor, S_0 is a scale parameter, S_u is a lower bound strength (of the largest feasible cracked particle), N_0 is the number of particles per unit volume, and f represents the fraction of "eligible" particles that participate in the fracture process.

Given the stress distribution within the plastic zone, the failure probability of the structure may be ascertained from Eq. (3) by determining S_0, S_u, N_0 and m from quantitative measurements of the particle size distribution and by independently evaluating f (11). Solutions to this problem, for cleavage fracture ahead of a rounded notch and ahead of a sharp crack, are compared below. The sharp crack solution has been presented in detail elsewhere (11).

III. STRESS FIELDS AHEAD OF A ROUNDED NOTCH

Available numerical results (10,26,27) for the stresses around notches are limited in scope and insufficient for the statistical modelling of fracture. Approximate analytic forms are thus evaluated in the present section, as a basis for subsequent statistical analysis. For this purpose, we consider a notch of depth a, root radius ρ and included angle $\pi/4$, subjected to a nominal (pure) bending stress (Fig. 2):

$$\sigma_{nom} = \frac{3PL}{B(W - a)^2} \quad , \quad (5)$$

where P is the applied load, L is the loading span, and B and W are the test piece thickness and width, respectively. For fully plastic conditions, the stress field in plane strain can be deduced from the slip-line field about the notch using characteristic lines of maximum shear stress defined by α = constant and β = constant (16) (Fig. 2). The upper and lower boundaries of the plastic zone are $\alpha = -\zeta$ and $\beta = \zeta$, where ζ decreases from $\pi/4$ to $\pi/16$ as general yield is approached. The principal axes coincide with the cylindrical coordinates (9):

$$r = \rho \exp (\pi/2 + \omega) \quad , \quad (6)$$

$$\Theta = \alpha + \beta$$

$$\omega = \alpha - \beta$$

Hence, assuming that the von Mises criterion pertains, the maximum

principal stress at any point within the plastic zone can be expressed as (28):

$$\sigma_1 = \frac{2}{\sqrt{3}} \left[\bar{\sigma} + \int_{\rho}^{r} \frac{\bar{\sigma}'}{r'} \, dr' \right] \quad . \tag{7}$$

Contours of constant σ_1 can be represented as circular arcs about the notch center, as illustrated in Fig. 2. For a non-hardening material, it follows that:

$$\frac{\sigma_1}{\sigma_0} = \frac{2}{\sqrt{3}} \left(1 + \ln \frac{r}{\rho} \right) \quad . \tag{8}$$

For a hardening material, the stresses may be derived from the distribution of equivalent strain ($\bar{\epsilon}$) directly below the notch root, because this strain is only weakly dependent upon the degree of hardening. Trends with r/ρ obtained for a linear work hardening material using finite elements are summarized in Fig. 3 (10). Expressions for $\bar{\epsilon}$, in regions close to the notch tip, indicate the following analytic approximations:

$$\bar{\epsilon} = \bar{\epsilon}_t \exp[- c_1(\frac{r}{\rho} - 1)] \quad , \qquad\qquad r < r_c \tag{9a}$$

$$\bar{\epsilon} = \bar{\epsilon}_t \exp[- c_2 \cdot \frac{r}{\rho} + (c_2 - c_1) \frac{r_c}{\rho} + c_1] \quad , \; r \geq r_c \tag{9b}$$

where c_1 (≈ 2.25) and c_2 are constants, $r_c \approx 2.3\rho$ and $\bar{\epsilon}_t$ is the equivalent strain at the notch tip. Comparison with finite element results indicates (Fig. 3) that Eq. (9) describes actual behavior

over the spatial range up to $r \sim 4\rho$. Previous expressions (29) were valid only for $r \sim 2\rho$.

For a power hardening (incompressible nonlinear elastic) material, with work hardening exponent n, where

$$\bar{\varepsilon}/\varepsilon_0 = (\bar{\sigma}/\sigma_0)^n \quad , \tag{10}$$

Eqs. (6) and (9) may be combined to give:

$$\frac{\sigma_1}{\sigma_0} = D_1\left(\frac{\bar{\varepsilon}_t}{\varepsilon_0}\right) D_2\left(\frac{r}{\rho}\right) \quad ,$$

where

$$D_1 = \frac{2}{\sqrt{3}}\left(\frac{\bar{\varepsilon}_t}{\varepsilon_0}\right)^{1/n} \quad ,$$

and

$$D_2 = \exp\left(\frac{c_1}{n}\right)\left[\exp\left(-\frac{c_1}{n}\cdot\frac{r}{\rho}\right) + \ln\frac{r}{\rho} + \sum_{i=1}^{\infty}\frac{(-c_1/n)^i}{i!i}\left\{\left(\frac{r}{\rho}\right)^i - 1\right\}\right] \quad , \qquad r < r_c$$

$$D_2 = \exp\left(\frac{c_1}{n}\right)\left[\ln\frac{r_c}{\rho} + \sum_{i=1}^{\infty}\frac{(-c_1/n)^i}{i!i}\left\{\left(\frac{r_c}{\rho}\right)^i - 1\right\}\right]$$
$$+ \exp\left(\frac{c_2 - c_1}{n}\frac{r_c}{\rho} + \frac{c_1}{n}\right)\left[\exp\left(-\frac{c_2}{n}\cdot\frac{r}{\rho}\right) + \ln\frac{r}{r_c} + \sum_{i=1}^{\infty}\frac{(-c_2/n)^i}{i!i}\left\{\left(\frac{r}{\rho}\right)^i - \left(\frac{r_c}{\rho}\right)^i\right\}\right] \quad . \qquad r \geq r_c \tag{11}$$

where σ_0 and ε_0 are the uniaxial yield stress and strain, respectively.

The utility of Eq. (11) in describing the notch-tip stress distribution in a power hardening solid can be affirmed by comparison with numerical solutions (10,26,27), as summarized in Fig. 4. For subsequent reference, the variation in $\bar{\varepsilon}_t$ with nominal stress, and the locations of the peak stress and the elastic-plastic interface, derived from the finite element solution, are shown in Fig. 5.

IV. FRACTURE AT ROUNDED NOTCHES

For a non-hardening material, the active zone elemental volume, in which σ_1 is constant (Eq. (2)), can be defined for the notch field as:

$$\delta V = b[\pi - 4\zeta - 2 \ln(r/\rho)]r\delta r \quad , \tag{12}$$

where b is a characteristic dimension along the crack front (19). From Eq. (4), the number of eligible carbides per unit volume is:

$$\int_0^{\sigma_1} g(S)dS = fN_0\left(\frac{\ln(r/\rho) + s}{t}\right)^m \quad ,$$

where

$$s = 1 - \frac{\sqrt{3}}{2} \cdot \frac{S_u}{\sigma_0} \quad \text{and} \quad t = \frac{\sqrt{3}}{2} \cdot \frac{S_0}{\sigma_0} \quad . \tag{13}$$

The failure probability of individual elements can thus be expressed as:

9

$$\delta\varphi = 1 - \exp\left[- fN_0 b\left(\frac{\ln(r/\rho) + s}{t}\right)^m \left(\pi - 4\zeta - 2\ \ln(r/\rho)\right)r\delta r\right] \quad . \quad (14)$$

After differentiation, it can be seen that the elemental failure probability exhibits a maximum at a distance ahead of the notch tip. This dimension, given by $(d\delta\varphi = 0)$:

$$r_f^* = \rho \exp\left\{\frac{1}{4}\left[(\pi-4\zeta-2) - 2(m+s) + \sqrt{(\pi-4\zeta-2)^2 + 4(m+s)^2 + 8m}\right]\right\} \quad (15)$$

represents the location ahead of the notch tip where the initial cracking event is most probable. This occurs at a fracture stress:

$$\sigma_f^* = \frac{2}{\sqrt{3}}\ \sigma_0\ [1 + \ln(r^*/\rho)] \quad . \quad (16)$$

For a power hardening material, the elemental and total failure probabilities become:

$$\delta\varphi = 1 - \exp\left[- fN_0 b\left\{\frac{D_1 D_2 - (S_u/\sigma_0)}{S_0/\sigma_0}\right\}^m (\pi - 4\zeta - 2\ \ln(r/\rho))r\delta r\right] \quad , \quad (17)$$

$$\Phi = 1 - \exp\left[- fN_0 b \int_\rho^{r_y}\left\{\frac{D_1 D_2 - (S_u/\sigma_0)}{S_0/\sigma_0}\right\}^m (\pi - 4\zeta - 2\ \ln(r/\rho))r\delta r\right] . (18)$$

Trends in the elemental failure probability with distance from the notch tip (Fig. 6) indicate that the most probable fracture site displaces away from the notch tip as the temperature increases. Specific trends in the critical distance r^* with temperature, deduced from Eq. (18), are plotted in Fig. 7a. Note that r^* coincides quite

10

closely with the location of the maximum value of the principal tensile stress, r_{max}.

Variations in the fracture load can also be deduced from Eq. (18), at various probability levels. Predictions of the load variation using values for the matrix variables pertinent to AISI 1008 steel are presented in Fig. 8, and compared with experimental data (Section VI).

V. FRACTURE AHEAD OF A SHARP CRACK

At the lowest temperatures, the plastic zone is small and the most probable cracking event occurs close to the elastic-plastic interface. Consequently, the extension of a sharp crack has been analyzed in terms of a linear elastic field (30) that best represents the variation in local crack tip stresses in that region. An asymptotic lower bound estimate of K_{Ic} results (11). Conversely, at higher temperatures approaching the ductile/brittle transition region, the most probable cracking event resides well within the plastic zone. Fracture behavior is then most adequately described in terms of the near-tip HRR nonlinear elastic stress distribution (31,32), with stresses truncated at roughly two crack tip displacements ($r < 2\delta$) from the tip due to crack tip blunting (9,33).

As the maximum tensile stresses are reached within $r \sim 2\delta$, stresses are progressively decreased over dimensions ahead of the tip comparable with the microstructurally relevant size-scales. The site

11

of the initial cracking event, i.e., the characteristic distance r_f^* where the elemental failure probability exhibits a maximum, thus reflects the mutual competition between behavior far from the tip, where the population of eligible cracked particles is large but stresses are low, and behavior close to the tip, where stresses are higher but the number of eligible particles is less. Based on the linear elastic and HRR fields, respectively, the characteristic distance is given by (11):

$$r_f^* = \frac{(5 - m)^2}{50\pi} \left[\frac{K_{Ic}}{S_u}\right]^2 \quad , \tag{19}$$

for the linear elastic field pertinent to low temperatures, and

$$r_f^* = \tilde{\sigma}^{n+1}\left[\frac{1-\nu^2}{I_n}\right]\left[\frac{2n+3-m}{2n+3}\right]^{n+1}\left[\frac{\sigma_0}{S_u}\right]^{n+1}\left[\frac{K_{Ic}}{\sigma_0}\right]^2 \quad , \tag{20}$$

for the nonlinear elastic HRR field pertinent to higher temperatures, where K_{Ic} is the fracture toughness, and I_n and $\tilde{\sigma}$ are dimensionless parameters from the HRR solution, tabulated in ref. 34. Typical trends in r_f^* are plotted in Fig. 7b. The corresponding fracture stresses are given by (11):

$$\sigma_f^* = \left[\frac{5}{5-m}\right] S_u \quad , \tag{21}$$

for the linear elastic field, and

12

$$\sigma_f^* = \left[\frac{2n + 3}{2n + 3 - m}\right] S_u \quad , \tag{22}$$

for the HRR field.

The fracture toughness, K_{Ic}, can also be predicted, when the total failure probability of material within the plastic zone is evaluated at the median level ($\Phi = 1/2$); at low temperatures:

$$K_{Ic} = \left[\frac{\ln 2}{1.35\eta \, fN_o b}\right]^{\frac{1}{4}} \left(\frac{S_o}{S_u}\right)^{m/4} S_u \quad , \tag{23}$$

and at higher temperatures:

$$K_{Ic} = \left[\frac{\ln 2}{\xi \eta fN_o b}\right]^{\frac{1}{4}} \left(\frac{S_o}{S_u}\right)^{m/4} S_u^{(1+n)/2} \, \sigma_o^{(1-n)/2} \quad , \tag{24}$$

where ξ and η are functions evaluated in ref. 26. Trends in predicted K_{Ic} values with temperature are presented in Fig. 9, pertinent to AISI 1008 steel.

VI. EXPERIMENTAL PROCEDURES

Experiments were performed on an AISI 1008 mild steel, of composition shown in Table I. The steel was austenitized at 920°C, air cooled, and spheroidized at 700°C for 7 days, to give a ferritic microstructure, with average grain size 25 μm, containing predominately spherical grain boundary carbides, with mean diameter ∿ 2 μm (termed L7 microstructure). The particle size distribution

13

Table I: Composition in wt.% of AISI 1008 Steel

C	Mn	P	S	Si	Fe
0.08	0.26	0.01	0.01	0.01	balance

for these carbides, together with the statistical parameters computed from the corresponding strength distribution, are shown in Fig. 10.

Variations in strength and ductility over the temperature range $-196^{\circ}C$ to $20^{\circ}C$, were assessed from uniaxial tensile tests (displacement rate 0.5 mm/min), and are shown in Fig. 11 (11). A work hardening exponent $n \simeq 4$ was obtained below $-70^{\circ}C$. Notched bend fracture tests were performed over a similar temperature range on 45° notched, 13 mm thick four-point bend test pieces (conforming to the Griffiths and Owen (10) test piece dimensions). Results, in terms of the variation in general yield (computed from the von Mises criteria) and fracture loads, are shown in Fig. 8. Plane strain fracture toughness K_{Ic} values, measured over the temperature range $-196^{\circ}C$ to $-70^{\circ}C$ on fatigue pre-cracked, single-edge-notched, 25 mm thick four-point bend specimens, are shown in Fig. 9 (11).

Optical and scanning electron microscopy was employed for metallographic examinations of microstructures and fracture surfaces, with an image analyzer used to evaluate grain and particle size distributions.

VII. RESULTS AND DISCUSSION

Model predictions of the variation in sharp crack (K_{Ic}) and rounded notch toughness with temperature for AISI 1008 steel have been presented (Figs. 8 and 9), assuming a maximum principal stress criterion with an effective fracture surface energy γ_p of 23 J/m^2 (35) and a fraction f of "eligible" carbides set at 5%. Predictions are shown for the median value ($\Phi = 0.50$) and indicate the statistical variation at each temperature ($\Phi = 0.01$ and 0.99).

The results confirm that the critical cracking event occurs some distance ahead of the notch or crack tip, consistent with fractographic evidence showing probable initiation sites to be particles located a few grain diameters from a crack tip (Fig. 12). The differences in the most probable location of this critical fracture event highlight the essential distinction between in cleavage fracture ahead of sharp cracks and rounded notches. In Fig. 13, the location of the critical fracture event at various temperatures ahead of a **sharp crack** is illustrated by superimposing the calculated values of σ_f^* and S_u on the crack tip stress distribution. Since the stress gradients are large and negative over the microstructural size scales relevant to the critical event, fracture is controlled by a statistical competition between particle crack nuclei of different sizes, i.e., the probability of finding an eligible particle crack is enhanced with increasing distance from the tip whereas the highest stresses are found with decreasing distance

15

from the tip. The more numerous fine particles can participate in the fracture process, provided they are situated close to the tip where they are subjected to the highest stresses.

The corresponding locations of the critical fracture event for the **rounded notch** at different temperatures are shown in Fig. 14. In contrast to the sharp crack the stress gradients are much shallower and indicate that the relevant local stresses and the probability of finding an eligible particle both increase with increasing distance from the tip. Statistically, there is now less competition between the location of the eligible crack nuclei and the highest stresses, with the result that the critical event occurs further from the tip. Moreover, due to this lack of statistical competition, the integrated failure criterion for the rounded notch will be associated primarily with the largest particles, consistent with early models of cleavage fracture under uniform stress fields (23) where it was postulated that fracture would initiate at the largest observable carbide.

The current model also implies, contrary to earlier analyses (14,17-21), that the fracture stress for cleavage cracking is not identical for failure ahead of sharp cracks and rounded notches. Although similar in magnitude, due to different sampling conditions for "eligible" particles within the process zone, the value of σ_f^* ahead of a notch decreases slightly with increasing temperature and approaches the lower bound value of S_u.

Such notions for failure ahead of sharp cracks and rounded notches are analogous for the phenomenon of ductile fracture, where

16

the local fracture processes involve void nucleation and growth around large primary particles (e.g., inclusions) and eventual coalescence via shear band localization from voids formed around numerous smaller particles (e.g., carbides) (36). Although the local failure criteria are now modelled in terms of a critical strain, exceeded over a dimension characteristic of the void initiating particles (9,37-39), ahead of sharp cracks where the strain gradients are extremely steep (9,33), it is still the finer and more numerous particles which dominate behavior as their spacings are comparable with the crack tip displacements (40). Conversely, ahead of rounded notches where the strain gradients are far shallower, the larger inclusions play the dominant role (41). This discussion serves to emphasize, as noted elsewhere (5-7,40), that the microstructural features responsible for fracture ahead of sharp cracks, i.e., that control plane strain fracture touchness, may not necessarily be those responsible for fracture ahead of rounded notches or in smooth samples; an important consideration when contemplating correlations between K_{Ic} and either Charpy toughness or tensile ductility.

VIII. SUMMARY AND CONCLUSIONS

A weakest link model for transgranular cleavage fracture has been applied to the problem of brittle crack extension from a rounded notch and from a sharp crack in single phase microstructures containing a known distribution of particles acting as a potential

17

crack nuclei. The model, which considers the probability of failure in constant stress elements within the plastic zone, is shown to predict the lower shelf rounded notch fracture load and sharp crack fracture toughness K_{IC}, as a function of such variables as temperature, flow stress, work hardening exponent, and the size distribution of particles.

The analysis provides a natural definition of the "characteristic distance" as the radial dimension from the crack or notch tip where the initial cracking event is most probable. For failure ahead of a sharp crack, where the stress gradients are large and local stresses **decrease** with progressively increasing distance from the tip (over microstructurally relevant dimensions), statistical competition exists between the decreasing stresses and an increasing probability of finding an "eligible" particle within the plastic zone with increasing distance from the tip. Computations suggest an approximately constant characteristic distance at stresses from 20 to 50% larger than the strength S_u of the largest observable particle. Conversely, for failure ahead of a rounded notch, where the stress gradients are shallow and local stresses increase slightly with increasing distance over the majority of the plastic zone, characteristic distances are found to be much larger and to increase sharply with temperature. The most probable initial cracking event is now expected to occur close to the point of maximum stresses, at a fracture stress σ_f^* **lower** than for the sharp crack. The value of σ_f^* in this case is found to approach S_u at higher temperatures.

Such analysis illustrates the essential differences between brittle fracture ahead of sharp cracks and rounded notches. Due principally to the weakly positive stress gradient over microstructurally-relevant dimensions ahead of the notch, the fracture process is dominated by the larger, lower strength particles. Fracture ahead of the sharp crack, on the other hand, is influenced additionally by the more numerous finer particles, as stresses are largest in the immediate vicinity of the tip.

ACKNOWLEDGMENTS

REFERENCES

1. ASTM A370-77, in "Standard Methods and Definitions for Mechanical Testing of Steel Products," 1983 Annual Book of ASTM Standards, Section 3, American Society for Testing and Materials, Philadelphia, PA, 1983, pp. 1-56.

2. ASTM E399-83, in "Standard Test Method for Plane Strain Fracture Toughness of Metallic Materials," ibid., pp. 518-53.

3. ASTM E813-81, in "Standard Test Method for J_{Ic}, a Measure of Fracture Toughness," ibid., pp. 762-80.

4. Rolfe, S. T., and Barsom, J. M., Fracture and Fatigue Control in Structures, Prentice-Hall, Englewood Cliffs, NJ, 1977.

5. Ritchie, R. O., in What Does the Charpy Test Really Tell Us?, A. R. Rosenfield et al., eds., American Society for Metals, Metals Park, OH, 1978, pp. 54-73.

6. Ritchie, R. O., Francis, B., and Server, W. L., Metallurgical Transactions A, vol. 7A, 1976, pp. 831-38.

7. Ritchie, R. O., and Horn, R. M., ibid., vol. 9A, 1978, pp. 331-41.

8. Floreen, S., Journal of Engineering Materials and Technology, Trans. ASME, Series H, vol. 100, 1978.

9. Rice, J. R., and Johnson, M. A., in Inelastic Behavior of Solids, M. F. Kanninen et al., eds., McGraw-Hill, NY, 1970, pp. 641-72.

10. Griffiths, J. R., and Owen, W. S., Journal of Mechanics and Physics of Solids, vol. 19, 1971, pp. 419-31.

11. Lin, Tsann, Evans, A. G., and Ritchie, R. O., ibid., vol. 34, 1986, in press.

12. McMahon, C. J., and Cohen, M., Acta Metallurgica, vol. 13, 1965, p. 591.

13. Smith, E., in Proceedings of Conf. on Physical Basis of Yield and Fracture, Institute of Physics, Oxford, UK, 1966, pp. 36-45.

14. Wilshaw, T. R., Rau, C. A., and Tetelman, A. S., Engineering Fracture Mechanics, vol. 1, 1968, pp. 191-211.

15. Knott, J. F., <u>Journal of Iron and Steel Institute</u>, vol. 204, 1966, pp. 104-11.

16. Hill, R., <u>The Mathematical Theory of Plasticity</u>, Clarendon Press, Oxford, UK, 1950.

17. Ritchie, R. O., Knott, J. F., and Rice, J. R., <u>Journal of Mechanics and Physics of Solids</u>, vol. 21, 1973, pp. 395-410.

18. Curry, D., and Knott, J. F., <u>Metal Science</u>, vol. 13, 1979, pp. 341-45.

19. Evans, A. G., <u>Metallurgical Transactions A</u>, vol. 14A, 1983, pp. 1349-55.

20. Beremin, F. M., <u>ibid.</u>, vol. 14A, 1983, pp. 2277-87.

21. Wallin, K., Saario, T., and Törrönen, K., <u>Metal Science</u>, vol. 18, 1984, pp. 13-6.

22. Hou Chun-xiao, Cai Qi-gong, Su Yi, and Zheng Xiu-yuan, in <u>Advances in Fracture Research '84</u>, Proc. Sixth Int. Conf. on Fracture, New Delhi, India, Dec. 1984, S. R. Valluri et al., eds., Pergamon Press, Oxford, UK, vol. 2, 1984, pp. 1415-22.

23. Curry, D., and Knott, J. F., <u>Metal Science</u>, vol. 12, 1978, pp. 511-4.

24. Matthews, J. R., Shack, W., and McClintock, F. A., <u>Journal of American Ceramic Society</u>, vol. 59, 1976, p. 304.

25. Weibull, W., <u>Ing. Vetenskap. Akad. Handl.</u>, vol. 12, 1939, p. 153.

26. Owen, D. R. J., Nayak, G. C., Kfouri, A. P., and Griffiths, J. R., <u>International Journal for Numerical Methods in Engineering</u>, vol. 6, 1973, pp. 63-73.

27. Bradford, R., C.E.G.B. South Western Region Report No. SWR/SSD/S/1300/S/83, Central Electricity Generating Board, Bistol, UK, May 1983.

28. Lin, Tsann, Ph.D. Thesis, Dept. of Matls. Sci. & Min. Engng., University of California, Berkeley, CA 94720, Jan. 1986.

29. Bates, R. C., and Santhanam, A. T., <u>International Journal of Fracture</u>, vol. 14, 1978, p. 501.

30. Williams, M. L., <u>Journal of Applied Mechanics</u>, vol. 24, 1957, pp. 109-14.

31. Hutchinson, J. W., <u>Journal of Mechanics and Physics of Solids</u>, vol. 16, 1968, pp. 13-31.

32. Rice, J. R., and Rosengren, G. R., <u>ibid.</u>, vol. 16, 1968, pp. 1-12.

33. McMeeking, R. M., <u>Journal of Mechanics and Physics of Solids</u>, vol. 25, 1977, pp. 357-81.

34. Shih, C. F., Division of Engineering, Brown University Report No. MRL E-147, Providence, RI, June 1983.

35. Gerberich, W. W., and Kurman, E., <u>Scripta Metallurgica</u>, vol. 19, 1985, pp. 295-98.

36. Cox, T. B., and Low, J. R., <u>Metallurgical Transactions</u>, vol. 5, 1974, p. 1457.

37. McClintock, F. A., <u>Journal of Applied Mechanics</u>, Trans. ASME Series E, vol. 35, 1968, pp. 363-71.

38. Mackenzie, A. C., Hancock, J. W., and Brown, D. K., <u>Engineering Fracture Mechanics</u>, vol. 9, 1977, pp. 167-88.

39. Ritchie, R. O., Server, W. L., and Wullaert, R. A., <u>Metallurgical Transactions A</u>, vol. 10A, 1979, pp. 1557-70.

40. Lee, S., Majno, L., and Asaro, R. J., <u>ibid.</u>, vol. 16A, 1985, pp. 1633-48.

41. Speich, G. R., and Spitzig, W. A., <u>ibid.</u>, vol. 13A, 1982, p. 2239.
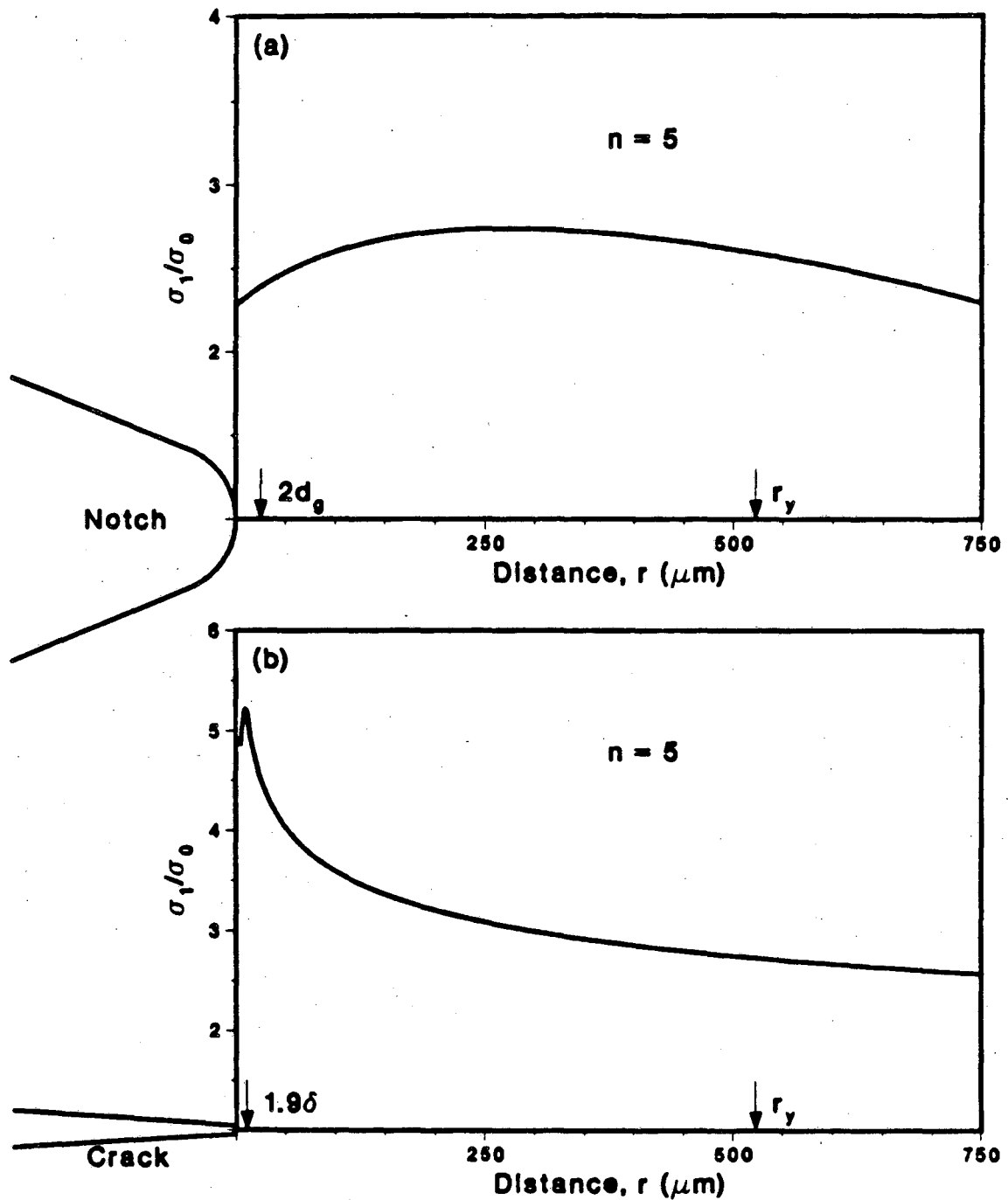
XBL 861-13

Fig. 1. Distribution of maximum principal stress, σ_1, normalized by the flow stress, σ_0, as a function of radial distance ahead of a rounded notch (root radius $\rho = \pi/4$) and a sharp crack. Note how the stress gradient is positive over the majority of the plastic zone size r_y for the notch, with the peak stress occurring many grain diameters, d_g, from the tip. For the crack, the stress gradient is sharply negative with the peak stress occurring at a couple of grain diameters from the tip. Results computed for a mild steel at -120°C. δ is the crack tip opening displacement, n is the work hardening exponent.

23

$$r = \rho \, \textbf{exp} \, [\, (\pi/2) + \alpha - \beta \,]$$

$$\theta = \alpha + \beta$$
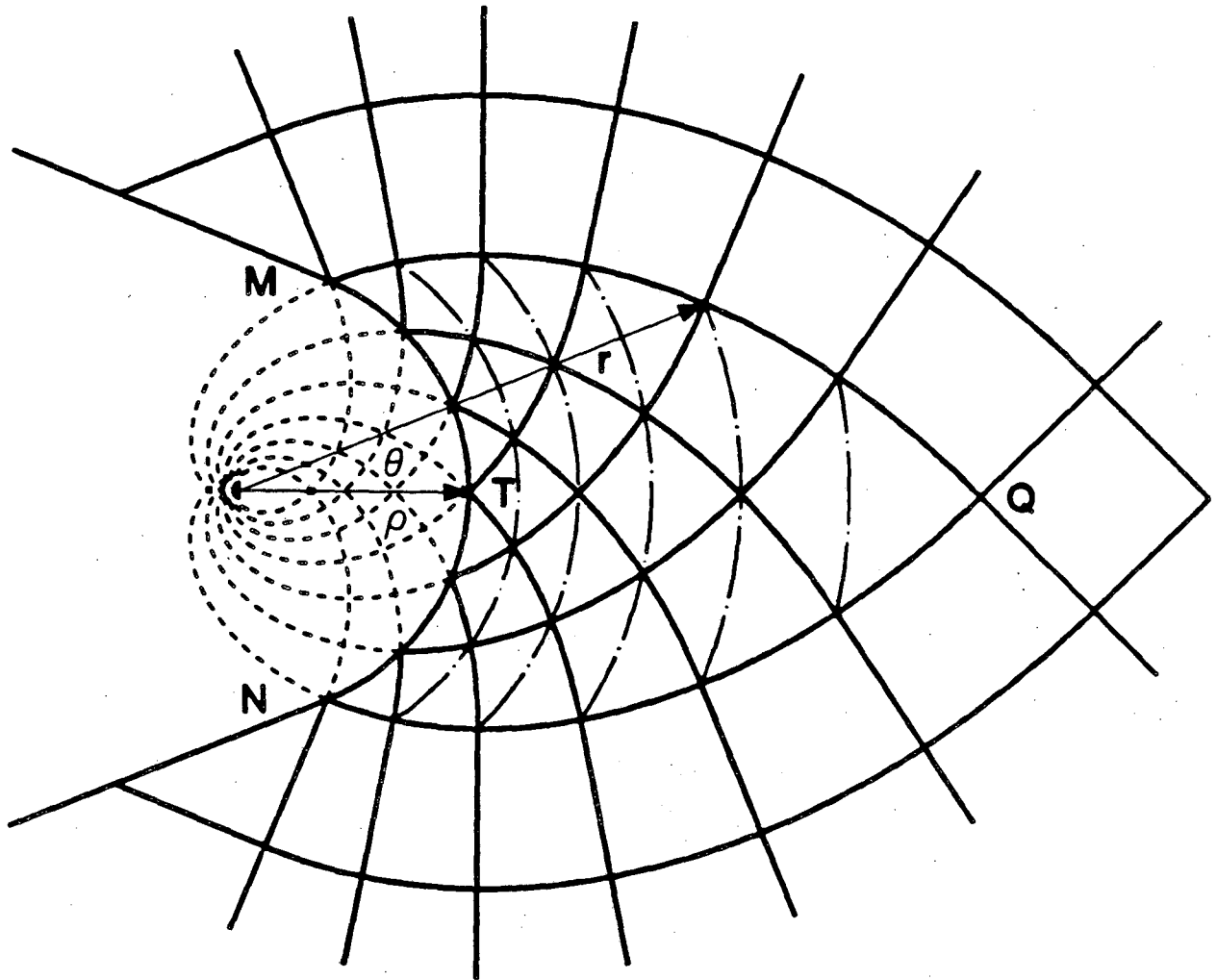
XBL 8512-5235

Fig. 2. Slip line field around a rounded notch with root radius ρ and included angle $\pi/4$. Four points shown can be expressed in characteristic α, β coordinates as M(- $\pi/16$, $7\pi/16$), N(- $7\pi/16$, $\pi/16$), T(- $\pi/4$, $\pi/4$), and Q(- $\pi/16$, $\pi/16$).
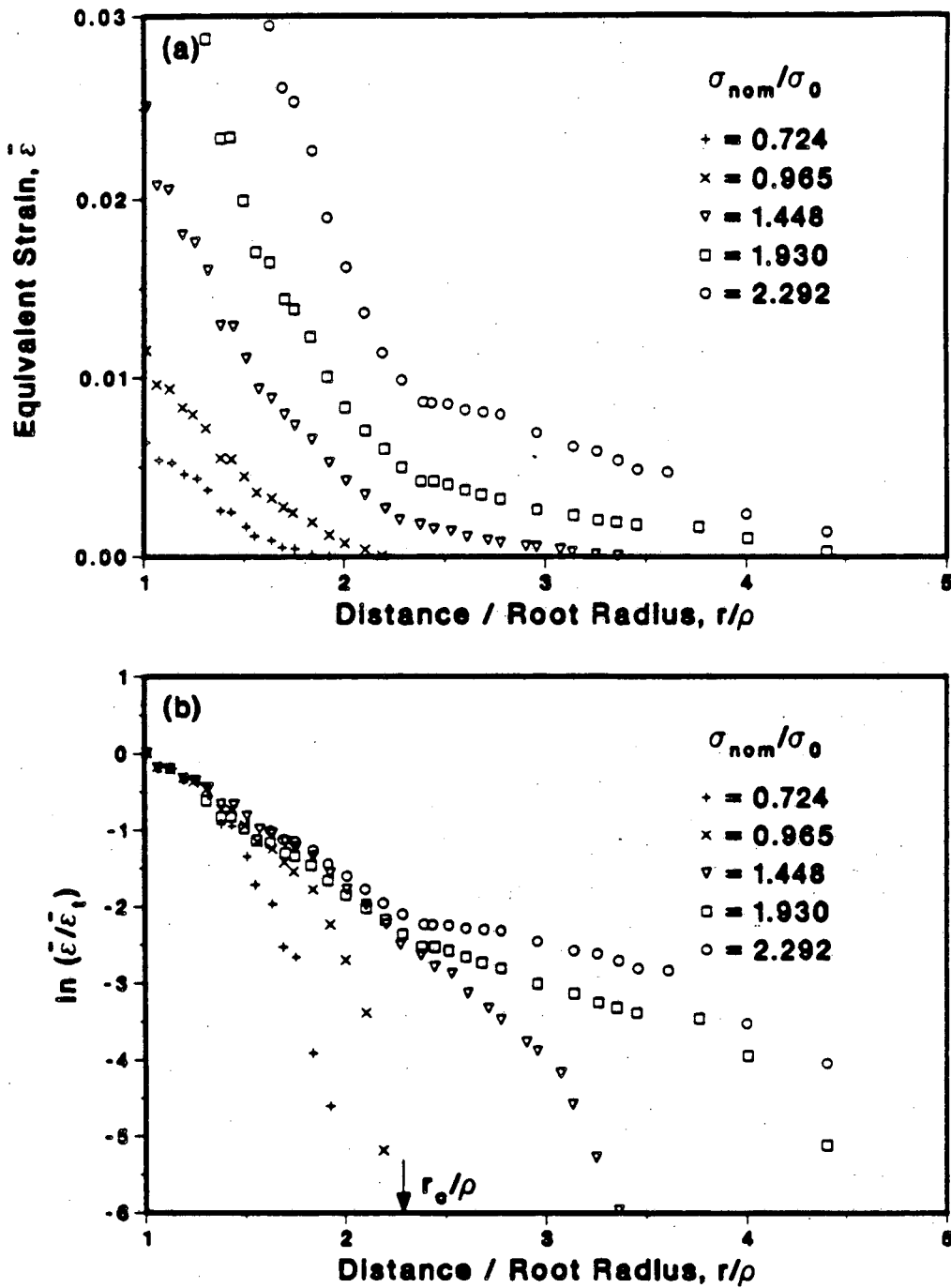
XBL 8512-5231

Fig. 3. Distributions of a) equivalent strain $\bar{\varepsilon}$, and b) $\ell n(\bar{\varepsilon}/\bar{\varepsilon}_t)$, as a function of normalized distance, r/ρ, from the center of a notch, of root radius ρ. Results are taken from the numerical computations of Griffiths and Owen (10) for a linear work hardening material with $\Delta\bar{\sigma}/\Delta\bar{\varepsilon} = E/120$. $\bar{\varepsilon}_t$ is the value of $\bar{\varepsilon}$ at the notch tip.
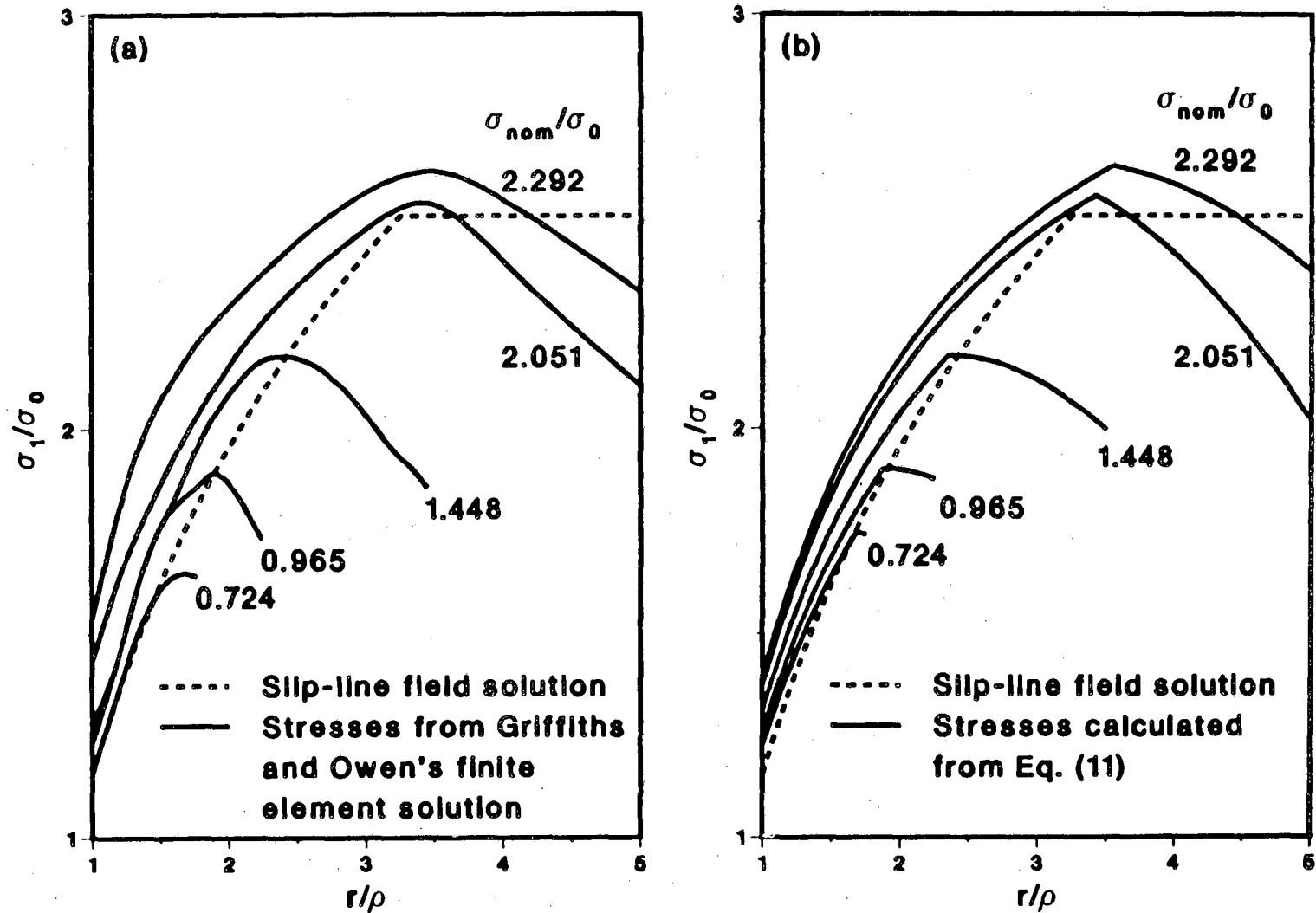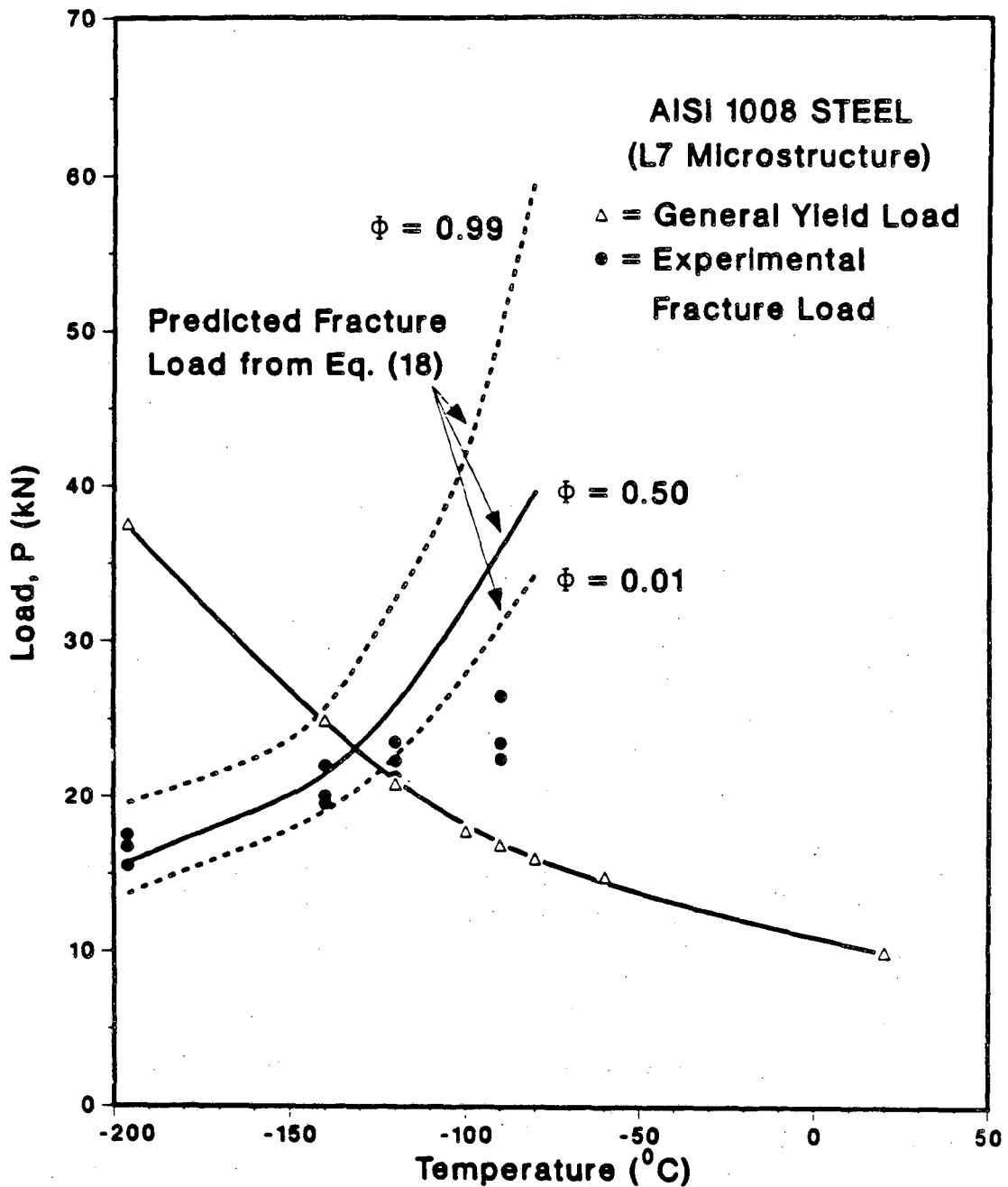
XBL 861-16

Fig. 4. Comparison of the maximum principal stress σ_1 distribution
ahead of a notch, of root radius $\pi/4$, in pure bending, as
computed from slip line field theory (16), from Griffiths
and Owen's numerical solutions (10) for a linear work
hardening solid with $\Delta\bar{\sigma}/\Delta\bar{\epsilon} = E/120$, and from the present
analytical solution for a power hardening solid with n = 10
(Eq. (11)).
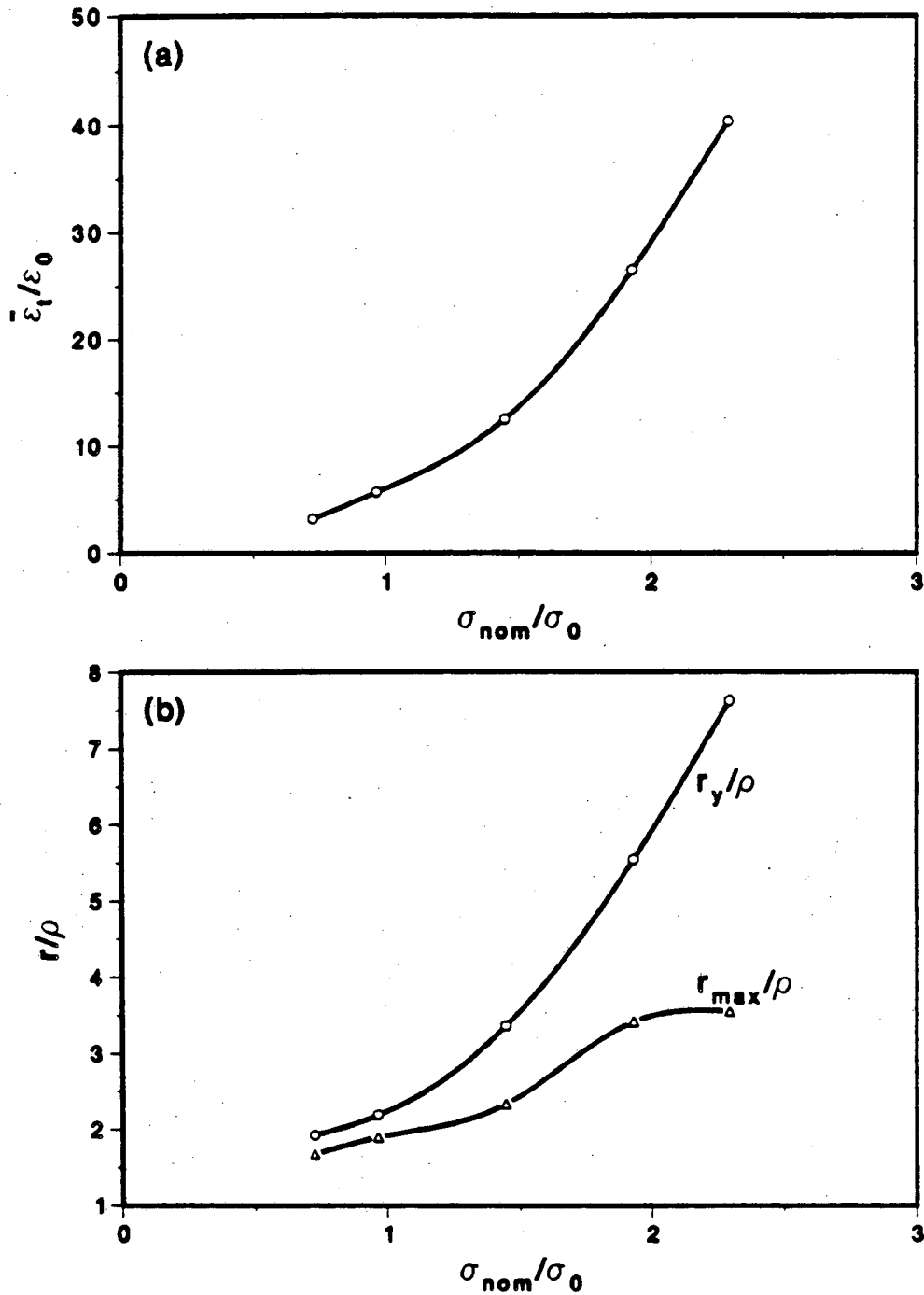
XBL 8512-5233

Fig. 5. Variations of a) the equivalent strain at the notch tip, $\bar{\varepsilon}_t$, normalized by the yield strain ε_0, and b) the location of the peak stress, r_{max}, and elastic-plastic interface, r_y, both normalized by the root radius ρ, as a function of the ratio of nominal bending stress to flow stress, σ_{nom}/σ_0 for a rounded notch in pure bending. Results are taken from the numerical computations of Griffiths and Owen (10) for a linear work hardening material with $\Delta\bar{\sigma}/\Delta\bar{\varepsilon} = E/120$.

27
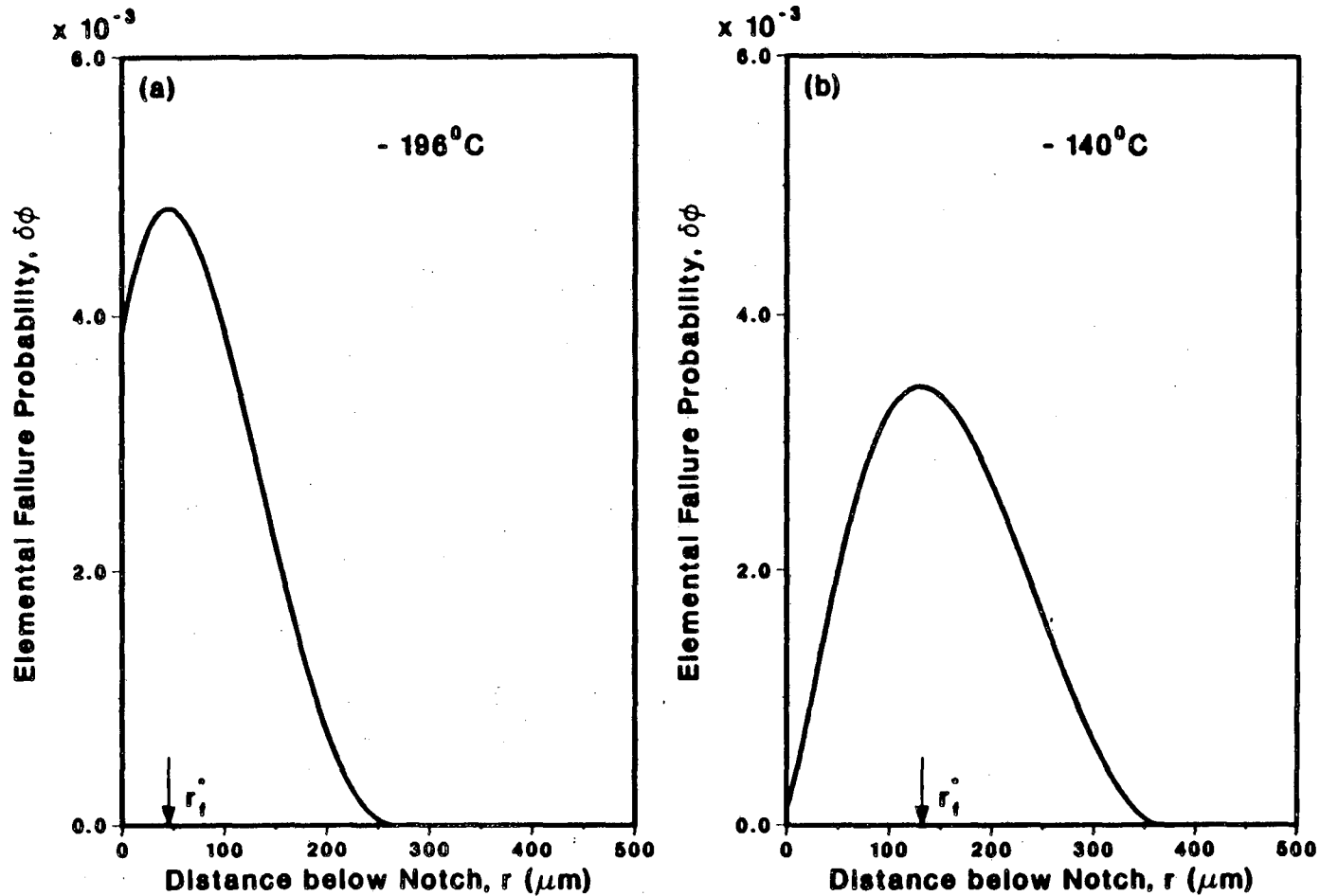
XBL 8512-5234

Fig. 6.   Distribution of elemental failure probabilities $\delta\varphi$ for
fracture ahead of rounded notch at a) -196°C and b) -140°C
when $\Phi = 0.50$. The characteristic distance r_f^*, representing
the location of the most probable initial cracking event, is
defined as the radial distance from the notch tip where
$\delta\varphi$ reaches a maximum, i.e, at $d\delta\varphi = 0$.
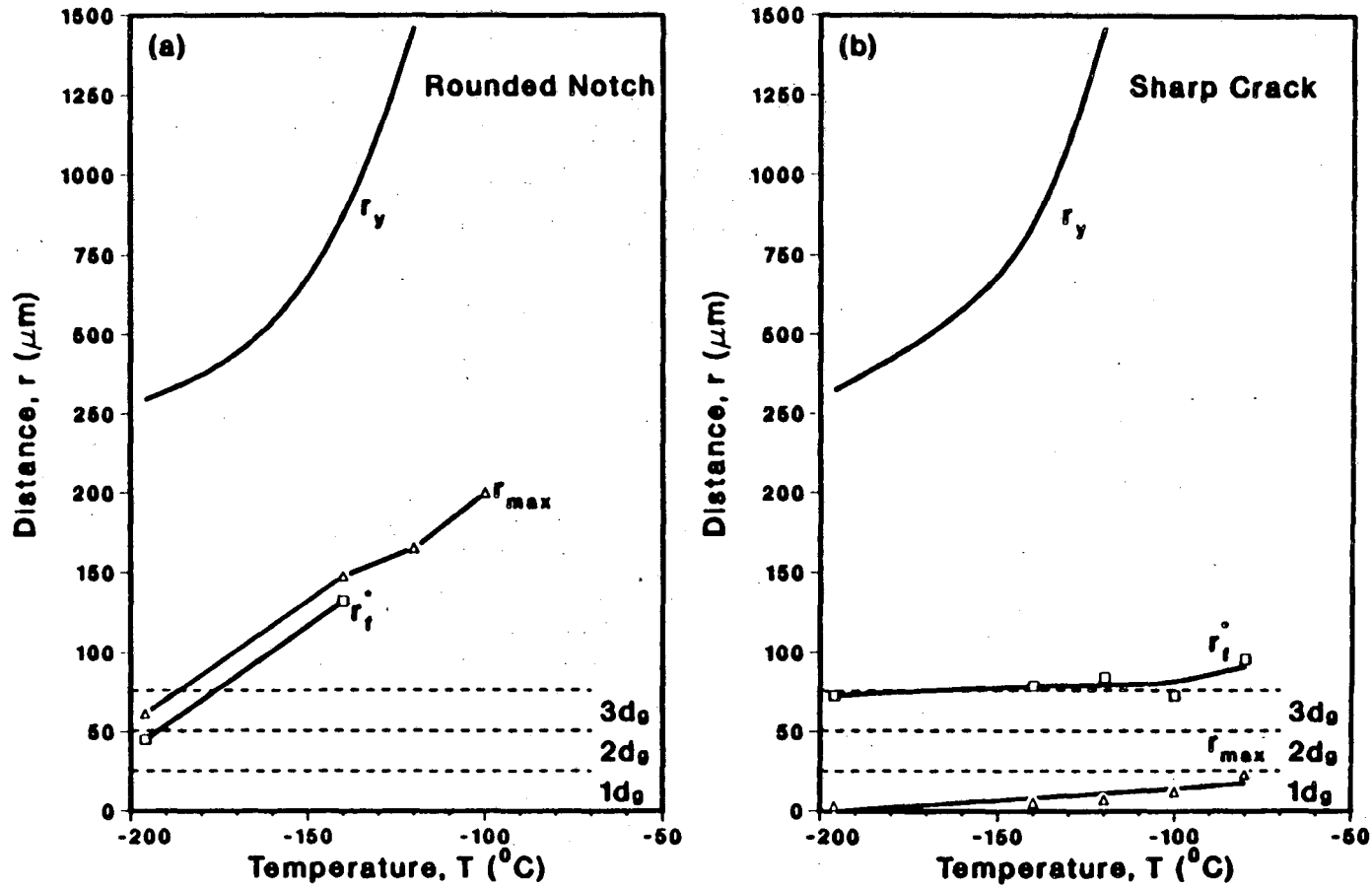
XBL 861-15

Fig. 7. Variation in location of maximum principal stress, r_{max}, elastic-plastic interface, r_y, and the most probable site of the initial cracking event, the characteristic distance r_f^*, as a function of temperature for brittle failure ahead of a) a sharp crack and b) a rounded notch, Results for AISI 1008 steel (L7 microstructure) with an average ferritic grain size of $d_g \approx 25$ μm.

Fig. 8. Experimentally measured variations in fracture load and general yield load with temperature in four-point single-edge-notched bend bars of AISI 1008 steel (L7 micro-structure). Also shown are predictions of the fracture load for catastrophic cleavage fracture from the statistical model (Eq. (18)), indicating median values (Φ = 0.50) and the anticipated statistical variation (Φ = 0.01 and 0.99).
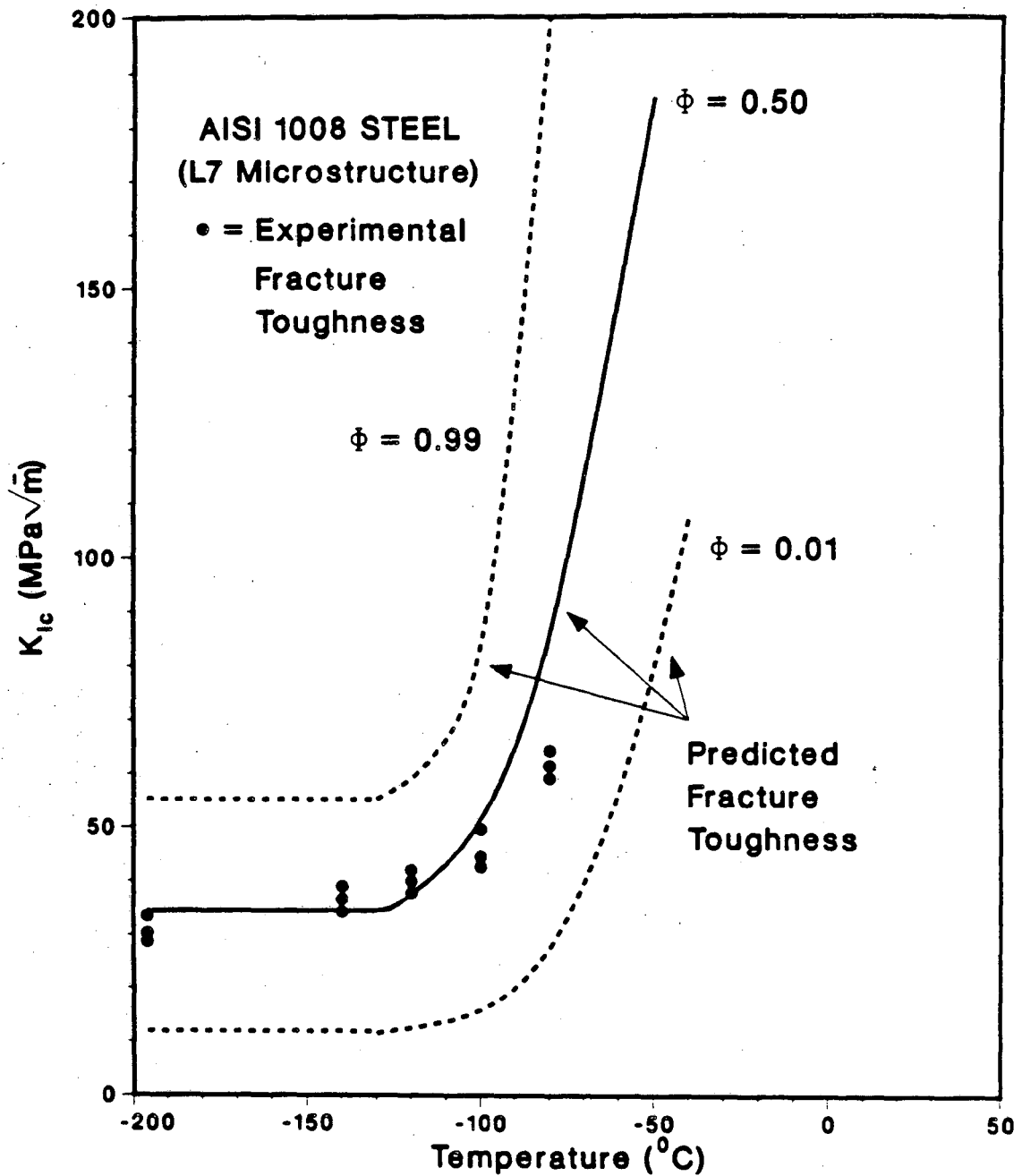
X8L 861-141

Fig. 9. Experimental measurements of the temperature dependence of plane strain fracture toughness K_{Ic} in AISI 1008 steel (L7 microstructure) based on pre-cracked four-point bend tests. Results above -100°C were computed from non-linear elastic J_{Ic} measurements. Also shown are the model predictions of K_{Ic} from Eqs. (23) and (24), indicating median values (Φ = 0.50) and the anticipated statistical variation (Φ = 0.01 and 0.99).
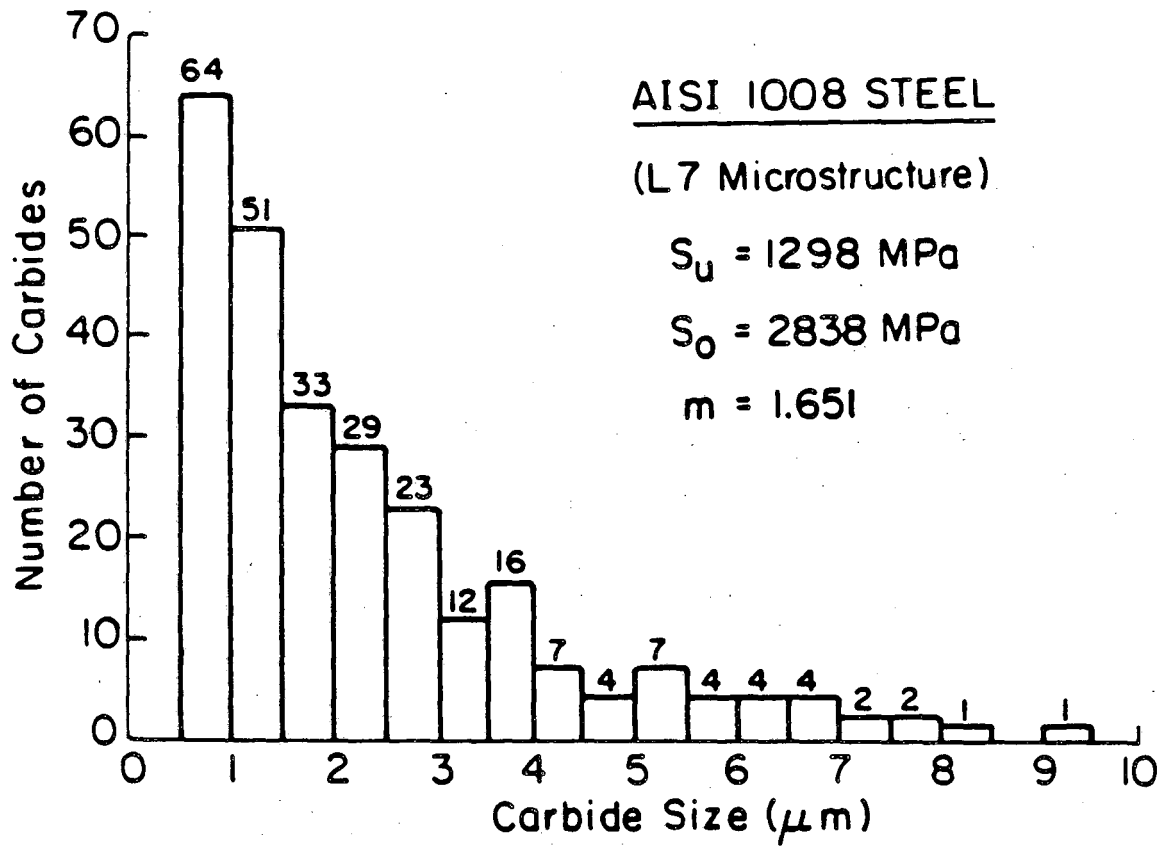
Fig. 10. Size distribution of carbides, measured in AISI 1008 steel after spheroidizing 7 days at 700ºC (L7 microstructure).
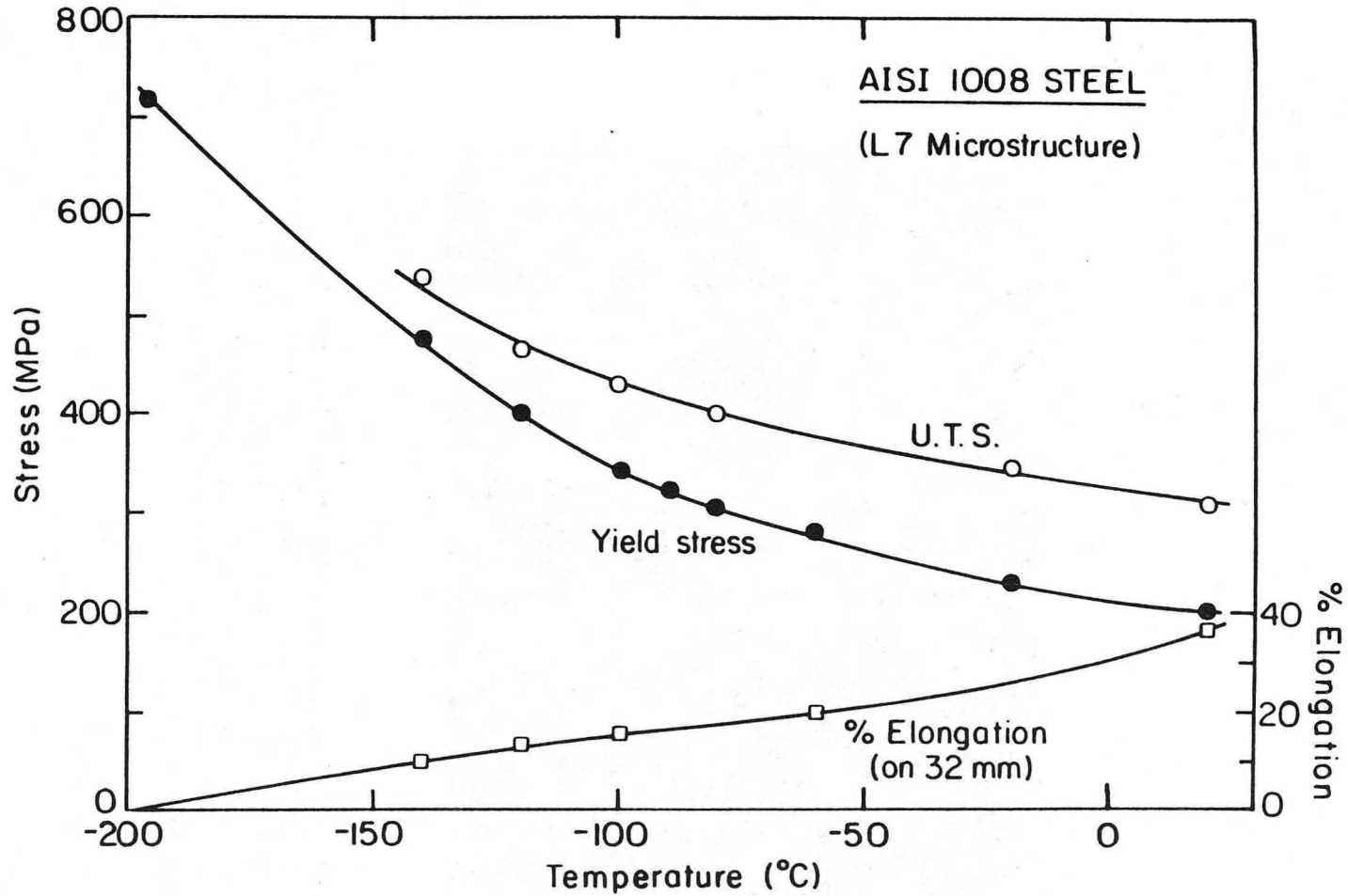
Fig. 11. Experimental measurement of the temperature dependence of uniaxial tensile properties of AISI 1008 steel (L7 micro-structure). Shown are the (lower) yield stress, U.T.S., and % elongation (on 32 mm gauge length).
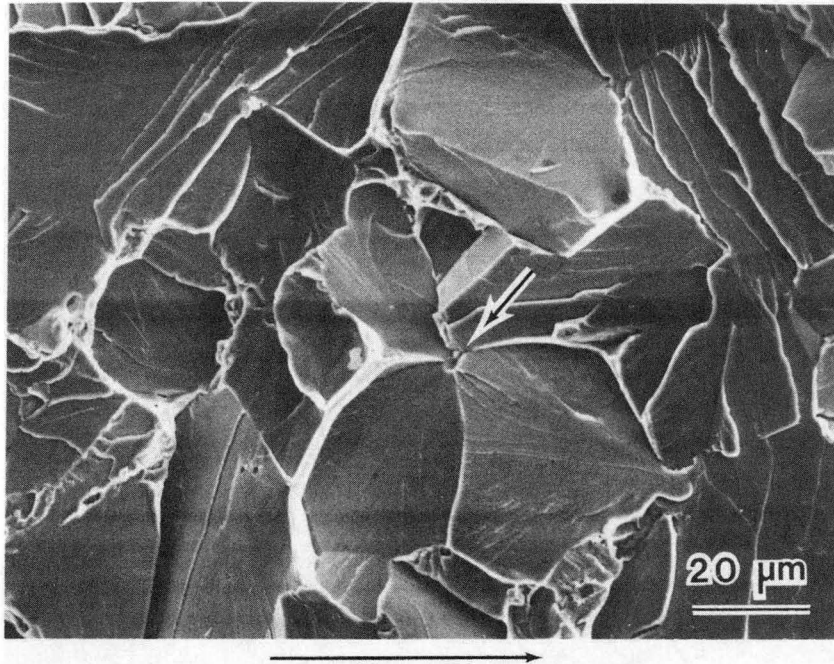
XBB 851-966A

Fig. 12. Scanning electron micrograph of cleavage fracture surface of AISI 1008 steel at -120°C showing possible initiation site at grain boundary carbide **ahead** of a crack tip. Note how river markings on surrounding cleavage facets point both in the direction of crack growth (indicated by arrow) and back towards the crack tip.
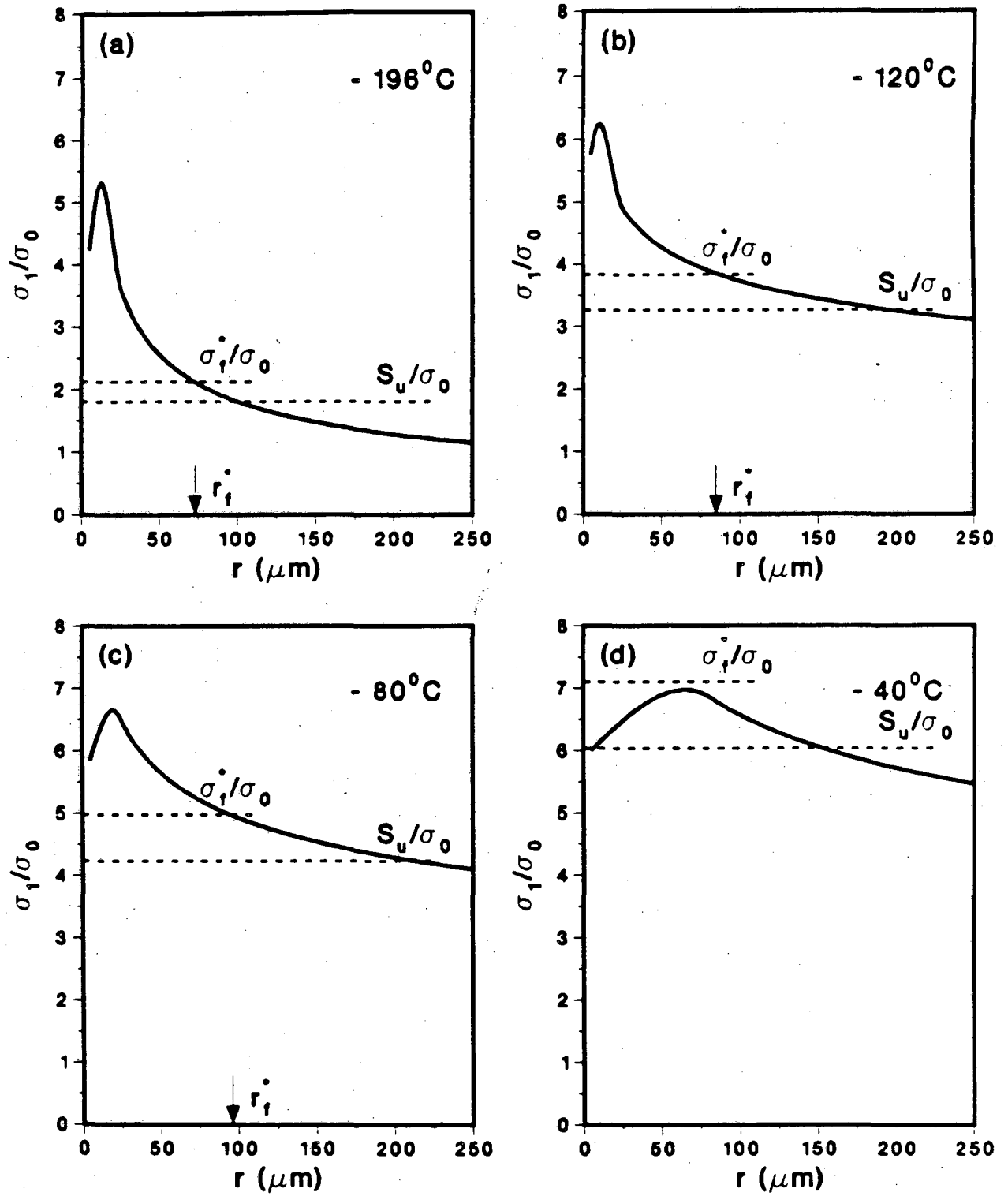
Fig. 13. Illustration of the local failure criteria for cleavage
fracture ahead of a sharp crack at a) -196°C, b) -120°C, c)
-80°C, and d) -40°C. Fracture occurs when $\sigma_1 > \sigma_f^*$. Above
-40°C, **catastrophic** fracture is not predicted as $\sigma_1 \ngtr \sigma_f^*$
over the characteristic distance.

XBL 861-140
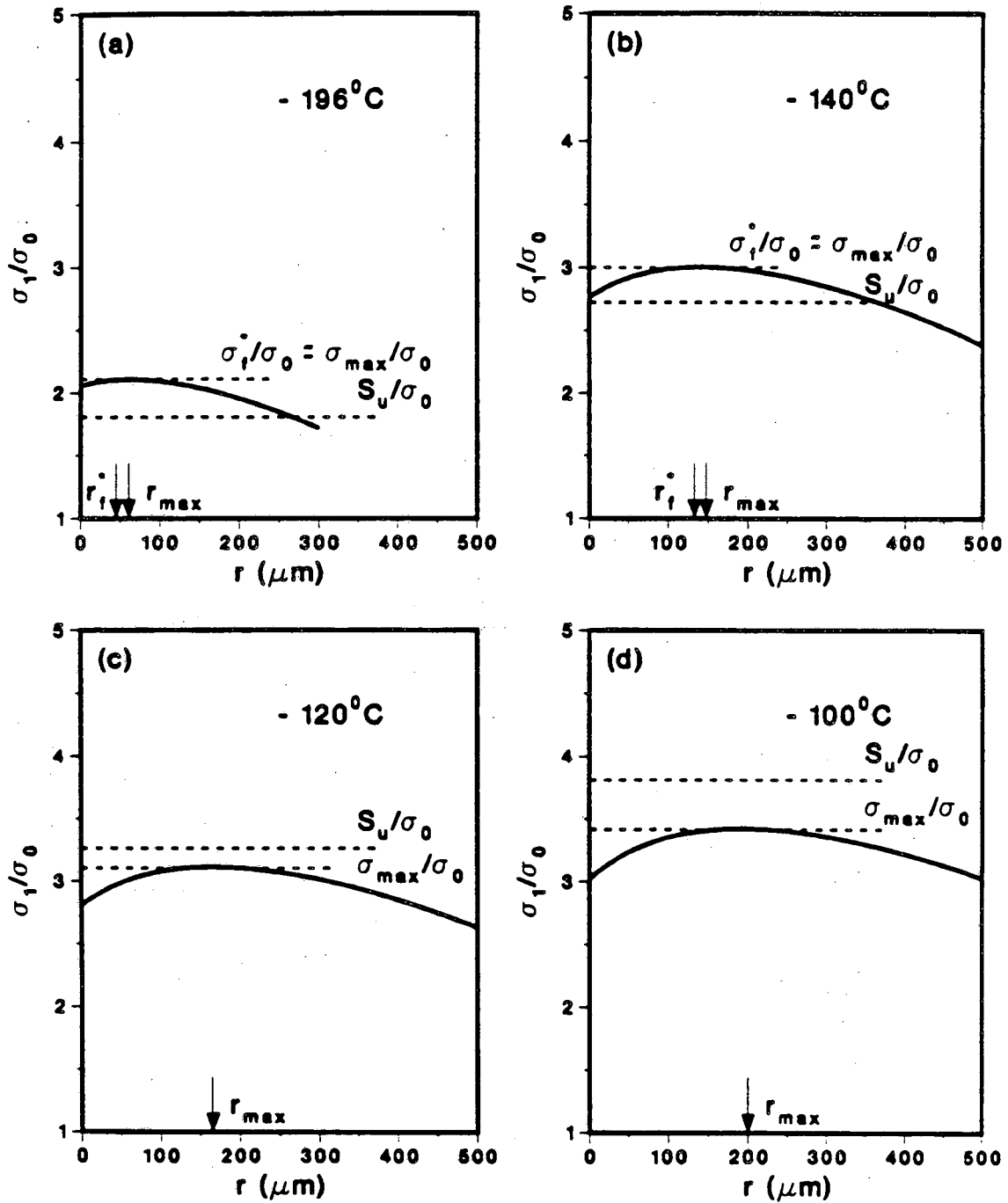
Fig. 14. Illustration of the local failure criteria for cleavage
fracture ahead of a rounded notch at a) -196°C, b) -140°C,
c) -120°C, and d) -100°C. Fracture occurs when $\sigma_1 > \sigma_f^*$,
approximately at the point of peak stress. Above -120°C,
catastrophic cleavage fracture is not predicted as $\sigma_1 \not\succ S_u$
or σ_f^*.

36
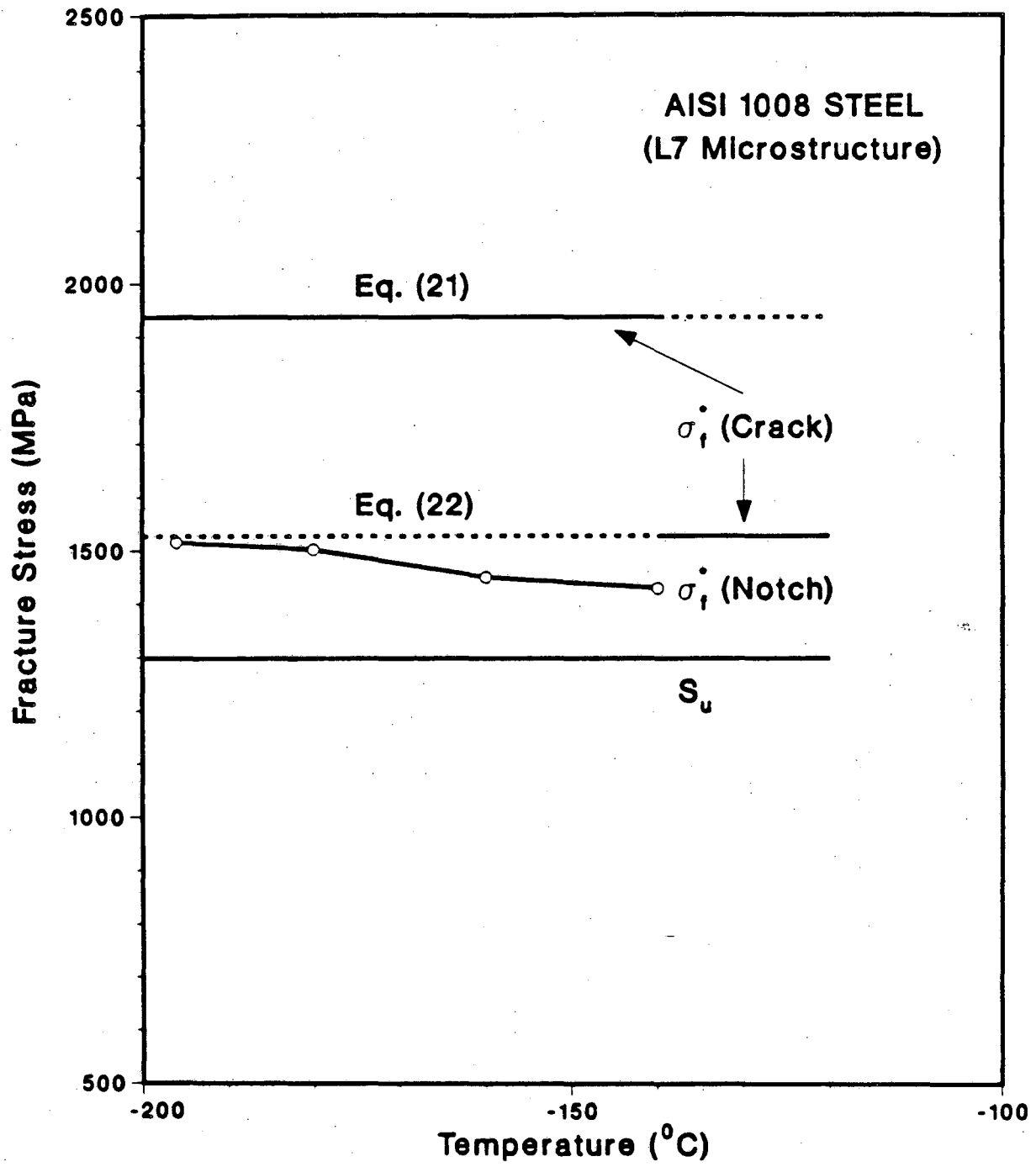
XBL 861-142

Fig. 15. Model predictions for the critical fracture stress for cleavage, σ_f^*, ahead of a sharp crack (Eqs. (21,22)) and a rounded notch (Eq. (16)) for AISI 1008 steel (L7 microstructure). S_u is the fracture strength of the largest observable particle.

37